



# Fatigue strength improvement in roller chain due to press fitting between pin and outer plate and between bush and inner plate

Ryoichi Saito<sup>a,\*</sup>, Nao-Aki Noda<sup>b,\*</sup>, Yoshikazu Sano<sup>b</sup>, Arata Miyagi<sup>b</sup>, Hisanori Tottori<sup>b</sup>

<sup>a</sup> ZEXUS CHAIN Corporation Kanto Works, 5110 Mikajiri Kumagaya-shi Saitama-ken 360-0843, Japan

<sup>b</sup> Mechanical Engineering Department, Kyushu Institute of Technology, 1-1 Sensuicho, Tobata-ku, Kitakyushu-shi, Fukuoka-ken 804-8550 Japan

## ARTICLE INFO

### Keywords:

Roller chain  
Fatigue strength  
FEM  
Fretting fatigue  
Nominal stress

## ABSTRACT

The press-fitting effect on the fatigue strength is studied experimentally with FEM for the plate/pin and for plate/bush since they control the whole strength of the roller chain. The results confirm that a relatively smaller press-fitting ratio is useful for improving the fatigue strength efficiently since it is highly productive. This observation suggests that if the damage caused by the currently used press fitting can be prevented, the fatigue strength of real roller chains can be greatly improved by increasing the fitting ratio. A newly defined nominal stress definition is proposed and confirmed to be useful for machine design.

## 1. Introduction

As shown in Fig. 1(a), the roller chain consists of a series of five components, that is, a pin, a bush, an inner plate, an outer plate, and a roller. Roller chains are commonly used to transmit mechanical power in many types of industrial machinery such as conveyors, motorcycles, and bicycles. Driving force is transmitted directly to the chain by meshing sprockets connected to the power source. Compared to belt drives, the transmission capacity is much higher, the slip is negligible, and the transmission efficiency is higher. Also, the length of the belt cannot be adjusted after operation has started, but the length of the roller chain can be adjusted as needed. Such advantages of the roller chain are utilized in a wide range of industrial fields such as steel, automobiles, chemistry, foodstuffs, and electronics.

Regarding the roller chain, lots of efforts have been done to improve the fatigue life by introducing high strength components and applying new technology to improve wear resistance [1–35]. Since the conventional wear testing requires huge amount of testing time/cost with a large variation of the results, a new wear testing machine consisting of only a few components was recently developed by the authors so that the time and cost can be reduced with a smaller variation of the results [31]. However, during the operation, sometimes fatigue failure still happened mainly at the outer/inner plate's holes where the bush and pin are press-fitted. In this way, it is known that the fatigue strength of roller chains is usually determined by the strength of the outer/inner plate having

press-fitted structures.

A well-known example of fitting fastening can be seen in the axles and wheels in railroad vehicles where fatigue fracture sometimes happened at the press-fitted portions of the axle. Therefore, lots of studies focused on the fracture of the axle [37–42] but no studies treated the wheel. Note that the pin of the roller chain corresponds to the railway axis, and the outer plate corresponds to the wheel. In roller chains, however, fatigue failure usually happened at the outer/inner plates corresponding to the wheel. In this way, since no studies are available, it is necessary to clarify the effect of the press-fitting on the fatigue strength of the plates.

Focusing on the press-fitted plate, an axisymmetric thick cylindrical plate with a press-fitted pin was initially analyzed. Then, the results showed that the press fitting reduces the stress amplitude and improves the fatigue limit [32–34]. Since the axisymmetric modelling cannot treat the uniaxial tension like Fig. 1, the three-dimensional FEM analysis was recently applied to discuss the shrink-fitted stress [35]. The authors analyzed the total structure of the roller chain in Fig. 1(a) to identify that the maximum and minimum stresses of press-fitted components during operation. Then, the results confirmed that the outer and inner plates are the most dangerous components of the real roller chains [30]. However, the fatigue strength of the roller chain has not been discussed yet considering the press-fitting effect. This is partly because the fatigue strength in Fig. 1(a) is largely affected by the slight manufacturing errors of each component.

\* Corresponding authors.

E-mail addresses: [ryoichi.saito@zexuschain.com](mailto:ryoichi.saito@zexuschain.com) (R. Saito), [noda.naoaki844@mail.kyutech.jp](mailto:noda.naoaki844@mail.kyutech.jp) (N.-A. Noda), [sano.yoshikazu029@mail.kyutech.jp](mailto:sano.yoshikazu029@mail.kyutech.jp) (Y. Sano), [miyagi.arata468@mail.kyutech.jp](mailto:miyagi.arata468@mail.kyutech.jp) (A. Miyagi), [tottori.hisanori731@mail.kyutech.jp](mailto:tottori.hisanori731@mail.kyutech.jp) (H. Tottori).

<https://doi.org/10.1016/j.ijfatigue.2022.107451>

Received 3 July 2022; Received in revised form 15 November 2022; Accepted 30 November 2022

Available online 5 December 2022

0142-1123/© 2022 The Authors. Published by Elsevier Ltd. This is an open access article under the CC BY-NC-ND license (<http://creativecommons.org/licenses/by-nc-nd/4.0/>).

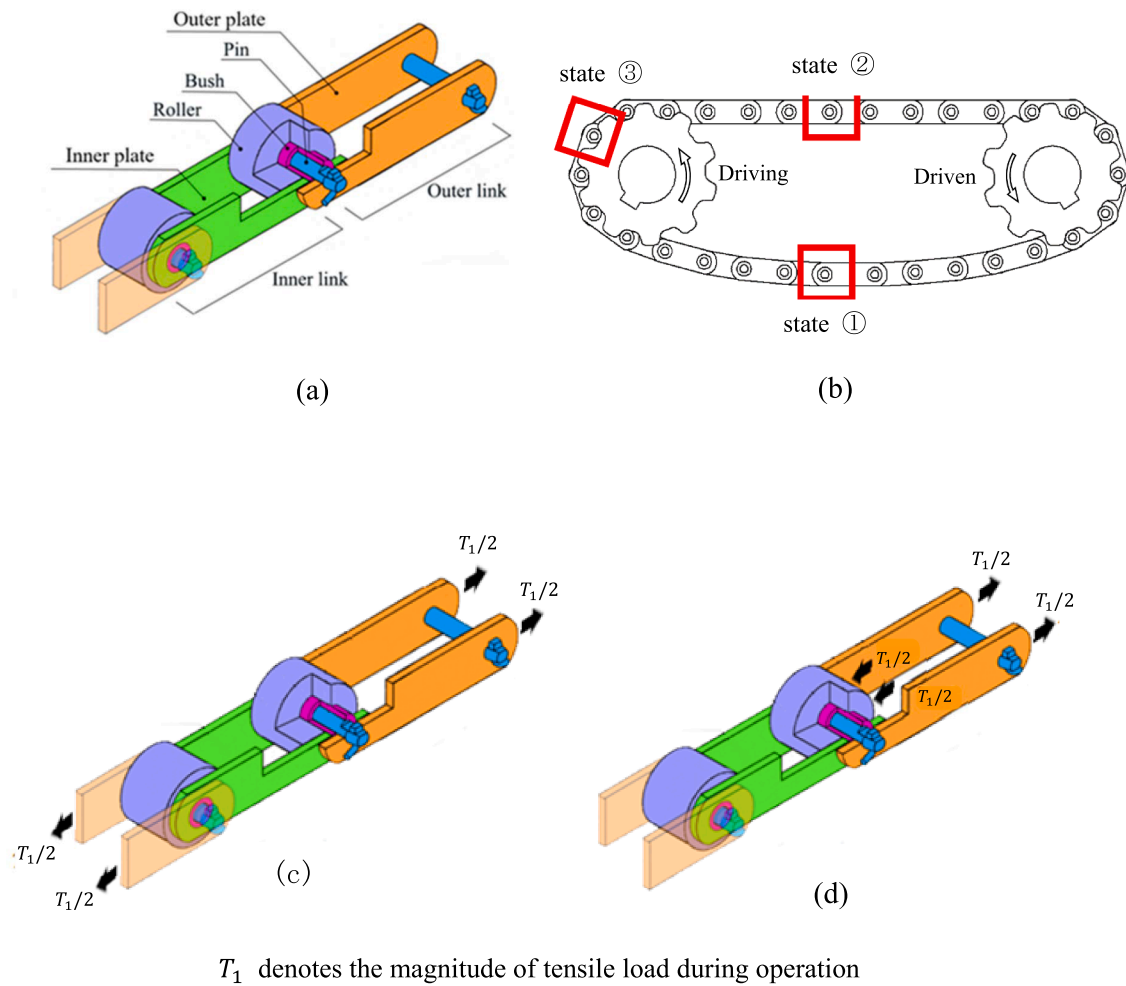


Fig. 1. Schematic illustration of the roller chain: (a) press-fitting state where no external force (state①). (b) roller chain drive system; (c) tensile state (state②); (d) sprocket-engaging state (state③).

In this paper, therefore, to clarify the press-fitting effect on the fatigue strength, two kinds of plate specimens in Fig. 2 will be used to conduct the fatigue experiment. Fig. 2(a) shows that two pins are press-fitted into the plate holes to investigate the outer plate in Fig. 1. Fig. 2(b) shows that two bushes are press-fitted into the plate holes to investigate the inner plate in Fig. 1. Then, the fatigue strength will be discussed by varying the press-fitting ratio with the aid of the finite element method (FEM). The final goal is to improve the fatigue strength of roller chains. Also, this paper will discuss smaller press-fitting ratio, which is desirable in the machine design to provide almost the same fatigue strength. This is because press-fitting structures can be manufactured more efficiently without scratch-like damage under such smaller press-fitting ratio.

## 2. Fatigue experiment to clarify the press-fitting effect on the fatigue strength

### 2.1. Fatigue test specimen geometries having press-fitting structures

The fatigue experiment should be conducted by using suitable specimens as well as under suitable cyclic loading. Fig. 2(a), (b) illustrate the test specimens toward improving the fatigue strength of the outer/inner plates of the real roller chain in Fig. 1. In Fig. 2(a), two pins are press-fitted into the plate holes to investigate the outer plate in Fig. 1. It should be noted that in Fig. 2(a), the two pins should be regarded as the specimen instead of the jig. In other words, the fatigue test specimen reflecting the outer plate consists of the two pins and the outer plate. In Fig. 2(b), two bushes are press-fitted into the plate holes

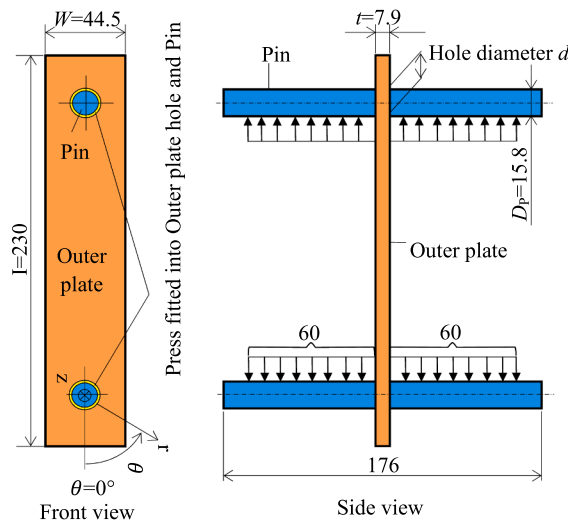
to investigate the inner plate in Fig. 1, and after that two pins are inserted into the bushes. In other words, the fatigue test specimen reflecting the inner plate consists of the two bushes, the two pins, and the inner plate.

In Fig. 2, notation  $d$  denotes the hole diameter of the outer plate,  $d_1$  denotes the hole diameter of the inner plate,  $W$  denotes the width of the outer/inner plates,  $t$  denotes the thickness of the outer/inner plates.  $D_p$  denotes the diameter of the pin,  $D_{BO}$  denotes the outer diameter of the bush, and  $D_{BI}$  denotes the inner diameter of the bush. As shown in the Fig. 2(a), the pin is press-fitted into the outer plate hole whose diameter  $d$  is smaller than the pin's outer diameter  $D_p = 15.8$  mm by the press-fit amount  $\delta = (D_p - d)$ . In the Fig. 2(b), the bush is press-fitted into the inner plate hole whose diameter  $d_1$  is smaller than the bush's outer diameter  $D_{BO} = 22.7$  mm by the amount  $\delta = (D_{BO} - d_1)$ . The pin's outer diameter  $D_p$  and the bush's inner diameter  $D_{BI}$  have a clearance of 0.5 mm.

Fig. 3 shows the preparation procedure of four components of those plate specimens, that is, the pin, the bush, the inner/outer plates. As shown in Fig. 3, the same plates and the same pins are used for the outer/inner plates but different hole diameters.

Table 1 shows the material properties of the components of the fatigue test specimens in Fig. 2, that is, the outer/inner plates, the pin and bush, all of which are quenched and tempered. The same materials are used in the real roller chain. Table 2 shows the chemical composition and microstructure of plates. Table 3 shows the press fitting ratio and dimensions for the fatigue test specimens in Fig. 2.

As shown in Table 3, in this study for Fig. 2(a), four kinds of press-fitting amount are provided as  $\delta = 0, 0.04, 0.08, 0.15$  mm to

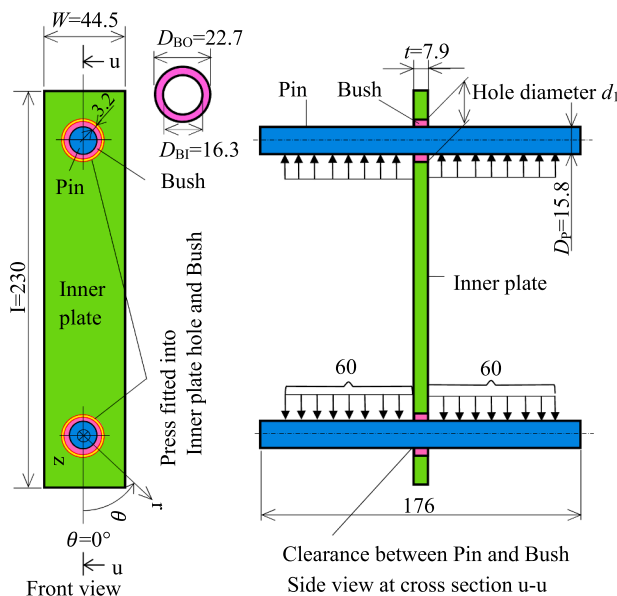


(a-1) Illustration



(a-2) Photograph

(a) Fatigue test specimen consisting of the pin and the plate reflecting the pin and outer plate in Fig. 1



(b-1) Illustration



(b-2) Photograph

(b) Fatigue test specimen consisting of the pin, the bush, the plate reflecting the bush, the pin and the inner plate, in Fig. 1

**Fig. 2.** Illustration of specimens (unit: mm) used to investigate the press-fitting effect on the fatigue strength where the angle  $\theta$  specifies the press-fitted position in Table 4, Table 6, Table 7.

investigate the press-fitting ratio  $\delta/D_p = 0, 2.5 \times 10^{-3}, 5.1 \times 10^{-3}, 9.5 \times 10^{-3}$ . The press-fitting ratio  $\delta/D_p = 9.5 \times 10^{-3}$  is currently used in real roller chains. When  $\delta/D_p = 0$ , to prevent the pin's come out, the pin is fixed at both ends with nuts as indicated in Fig. 4(a). The same prevention is used for the specimen in Fig. 2(b). For Fig. 2(b), four kinds of press-fitting amount are provided as  $\delta = 0, 0.04, 0.15, 0.25$  mm to investigate the press-fitting ratio  $\delta/D_{Bo} = 0, 1.8 \times 10^{-3}, 6.6 \times 10^{-3}, 11.0 \times 10^{-3}$ . The press-fitting ratio  $\delta/D_{Bo} = 6.6 \times 10^{-3}$  is currently used in real roller chains.

In this study, to clarify the effect of the press-fitting ratio accurately, the press-fitted parts are machined after heat treatment to provide the press-fitting ratio precisely. In this way, the press-fitted parts are machined after heat treatment to exclude the influence of heat treatment deformation. To reduce galling during the cold press-fitting, the pin's

diameter and the bush's outer diameter are oiled when press-fitted. When manufacturing real roller chains, the press-fit parts are machined before heat treatment. This is because machining of the press-fit parts after heat treatment requires machining of materials with high hardness.

## 2.2. Fatigue failure in real roller chain caused by difference of loading state

The fatigue experiment should be conducted under suitable cyclic loading as well as by using suitable specimens. The suitable cyclic loading conditions should be determined by reflecting the real roller chain in Fig. 1. As shown in Fig. 1, the applied loading states can be classified into three states, that is, "the press-fitting state ① in Fig. 1(a)",

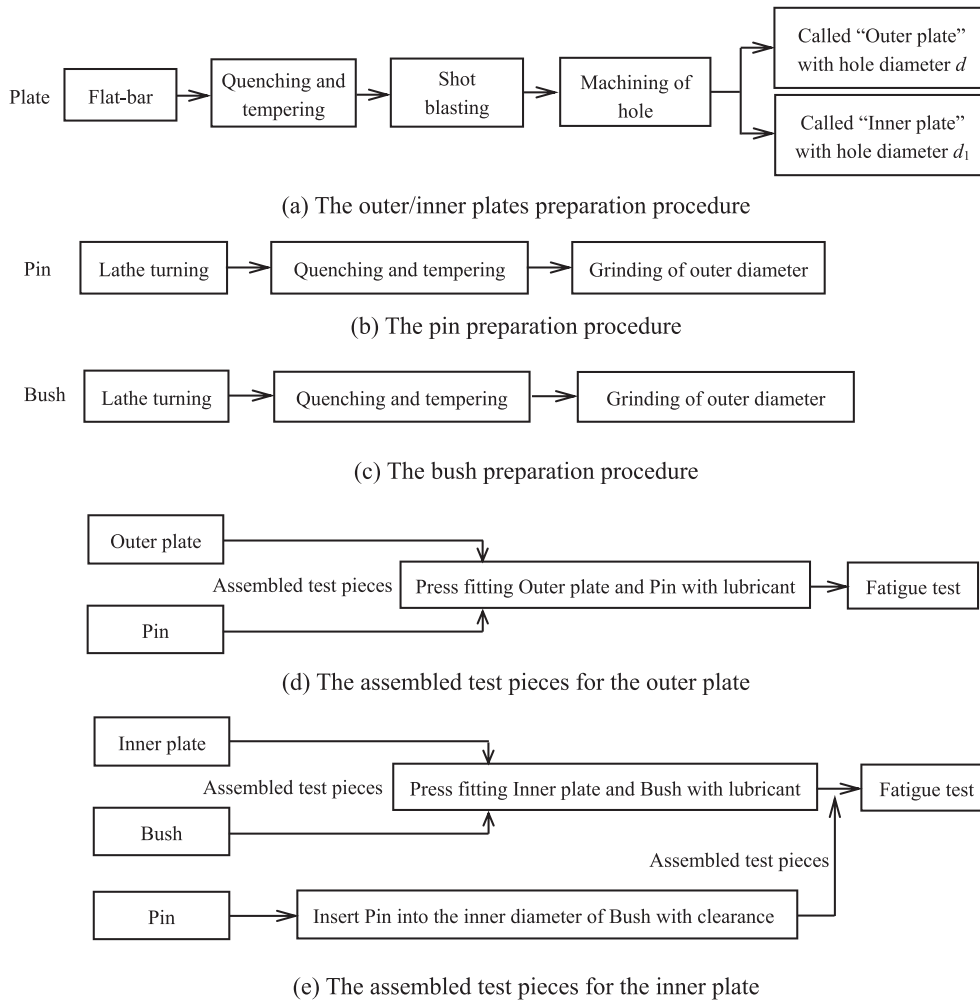


Fig. 3. Test pieces preparation procedure.

Table 1

Mechanical properties of the components of the fatigue test pieces in Fig. 2, which is also used in the real roller chain.

Parts	Material	Young's modulus E [GPa]	Poisson's ratio $\nu$	Yield stress $\sigma_y$ [MPa]	Tensile strength $\sigma_B$ [MPa]	Fatigue limit $\sigma_{w0}$ [MPa]	Friction coefficient $\mu$	Hardness [HRC]
Outer/ Inner plate	SS640 (Company standard)	206	0.3	970	1100	440	0.3	34.6
Bush	SCM435	206	0.3	1390	1666	666	0.3	48.4
Pin	SCM435	206	0.3	1080	1180	472	0.3	42.2

※ Fatigue limit  $\sigma_{w0}$  is estimated from  $\sigma_{w0}/\sigma_B = 0.4$  in reference [43].

“the tensile state ② in Fig. 1(c)” and “the engaging state ③ in Fig. 1(d)”.

Fig. 1(a) shows the state ① where no external force. In this state, the pin is pressed into the outer plate and the bush is pressed into the inner plate. This press-fitting state ① starts after the engaging state of the chain ③. Fig. 1(c) shows state ② where the tensile force is applied to the outer and inner plates. Pins are mainly subjected to shear loads from both plates, and bushes are mainly subjected to bending by the link plate. Fig. 1(d) shows engaging state ③ where the roller is pushed by the tooth of the sprocket. Fatigue failure in real roller chains occurs due to the stress variations caused by the difference between state ①, state ② and state ③. As shown in Appendix A, the authors previous analysis showed the stress amplitude generated in the inner/outer plates due to the difference between states ① and ② is the largest [30]. Therefore, the

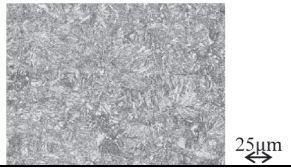
fatigue experiment should be conducted by considering the difference between the state ① and state ②, which generates the stress amplitude causing metal fatigue.

### 2.3. Loading conditions of fatigue test specimens having press-fitting structures

To clarify the press-fitting effect on the fatigue strength, the fatigue experiment is conducted under the cyclic loading  $F = F_{min} \sim F_{max}$ . Here, the minimum load  $F = F_{min}$  is corresponding to the press-fitting state ① where there is no external loading in Fig. 1. The maximum load  $F = F_{max}$  is corresponding to the tensile state ② in Fig. 1. Reflecting the real roller chain, the fatigue experiment should be conducted under pulsating

**Table 2**  
Chemical composition and microstructure of the outer and inner plates.

Chemical composition [%]	Heat treatment condition	Microstructure
C 0.28	Quenching	Into a batch type furnace at 870 °C for 80 min
Si 0.26		
Mn 1.41		
P 0.015		
S 0.012	Tempering	Into a batch type furnace at 510 °C for 90 min
Cr 0.17		
Mo 0.02		
Fe Other		



alternative loading. Considering the real operations, the maximum load  $F_{max}$  varies in the range  $F_{max} = 25 \sim 80\text{kN}$  when the minimum load  $F_{min}$  is fixed as  $F_{min} = 3\text{kN} \cong 0$ . Therefore, the stress ratio  $R = F_{min}/F_{max}$  varies depending on  $F_{max}$  in accordance with the real loading operation

**Table 3**  
Press fitting ratio and dimensions for the fatigue test specimens in Fig. 2.

Parts	Width $W$ [mm]	Thickness $t$ [mm]	Pin's diameter $D_p$ [mm]	Bush's outer diameter $D_{BO}$ [mm]	Bush's inner diameter $D_{BI}$ [mm]	Hole diameter $d$ [mm]	Hole diameter $d_1$ [mm]	$\delta = D_p - d$ [mm]	$\delta = D_{BO} - d_1$ [mm]	$\delta/D_p$ [ $\times 10^{-3}$ ]	$\delta/D_{BO}$ [ $\times 10^{-3}$ ]
Outer plate	44.5	7.9	15.8	-	-	15.80	-	0.00	-	0	-
	44.5	7.9	15.8	-	-	15.76	-	0.04	-	2.5	-
	44.5	7.9	15.8	-	-	15.72	-	0.08	-	5.1	-
	44.5	7.9	15.8	-	-	15.65	-	0.15	-	9.5	-
Inner plate	44.5	7.9	15.8	22.7	16.3	-	22.70	-	0.00	-	0
	44.5	7.9	15.8	22.7	16.3	-	22.66	-	0.04	-	1.8
	44.5	7.9	15.8	22.7	16.3	-	22.55	-	0.15	-	6.6
	44.5	7.9	15.8	22.7	16.3	-	22.45	-	0.25	-	11.0

of the real roller chain. By using the nominal stress newly defined in section 3.2, the minimum nominal stress is  $\sigma_{n \min} = 13\text{MPa}$  at  $F_{min} = 3\text{kN}$  and the maximum nominal stress varies in the range  $\sigma_{n \max} = 110 \sim 352\text{MPa}$  corresponding to  $F_{max} = 25 \sim 80\text{kN}$ . Then, the fatigue experiment is conducted at 9 levels in the range of the stress ratio  $R = \sigma_{n \min}/\sigma_{n \max} = 0.036 \sim 0.12$ .

2.4. Fatigue experiment to clarify the press fitting on the fatigue strength

In real roller chains, the maximum stress amplitude appears from the tensile loading state ② and the press-fitting unloading state ① in Fig. 1 during the operation [30]. Considering those two states, the fatigue experiment is conducted under pulsating cyclic tensile loading. Fig. 4 illustrates the testing jig, the fatigue test specimen and fatigue test machine. Here,  $D_1$  is the hole diameter of the testing jig. As shown in Fig. 4(a), the pin's outer diameter  $D_p = 15.8\text{mm}$  is inserted into the testing jig's hole diameter  $D_1 = 16.3\text{mm}$  in the test machine. After inserting the pin, nuts are used to tighten the pin's thread at both ends so as to set almost no clearance between the inner plate and the testing jig.

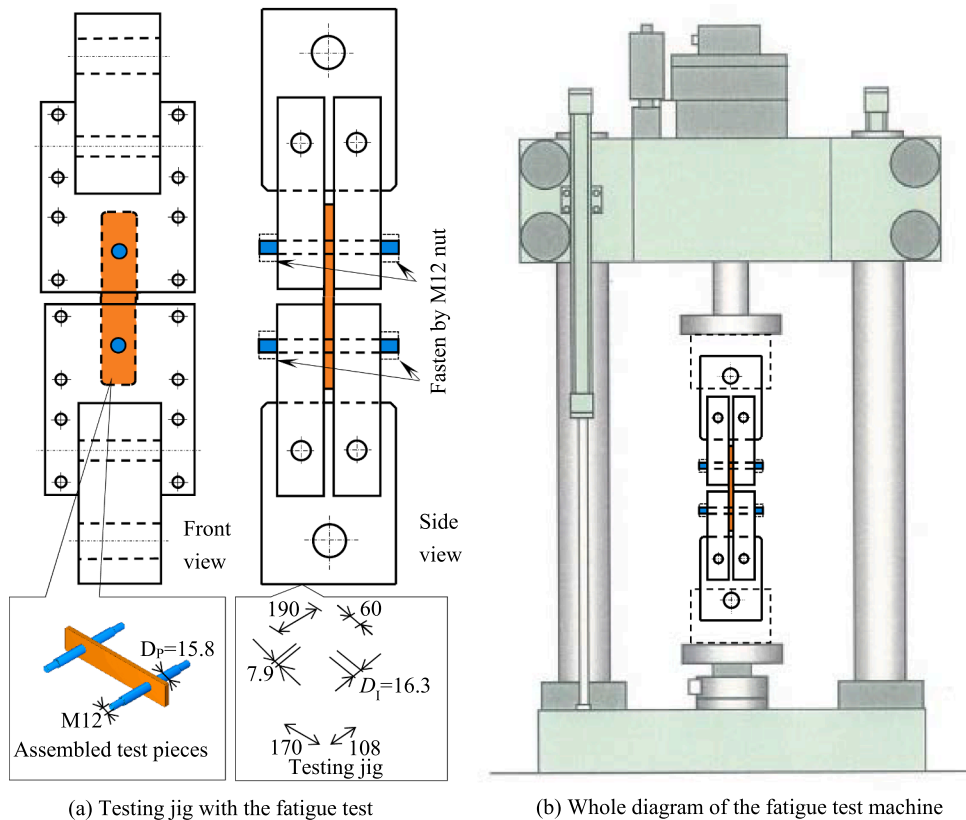


Fig. 4. Schematic illustration of the testing jig and fatigue test machine (unit: mm).



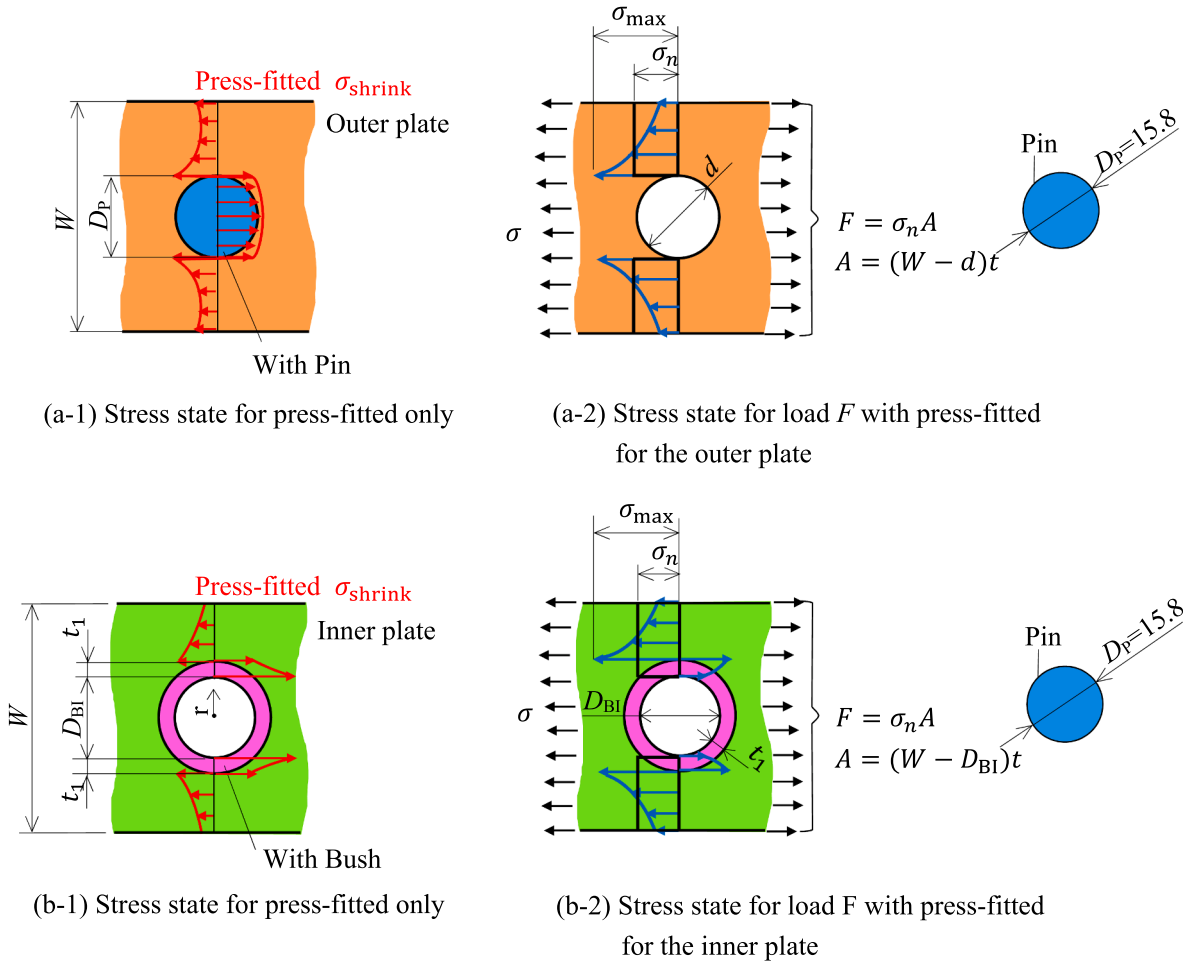


Fig. 5. Definition for nominal stress  $\sigma_n$  (unit: mm).

By tightening the nut with the torque about 10 Nm, an axial force of the pin becomes about 5.6kN and the stress becomes 28 MPa, which is negligibly small. This is the same for the inner plate's test specimens.

As shown in Fig. 4(b), the two testing jigs with test specimens are assembled to the fatigue test machine. The testing jig moves vertically by hydraulic motor of fatigue test machine. The test frequency was fixed as 10 Hz and the fatigue limit is evaluated at the number of cycles to failure  $N_f = 10^7$ . The fatigue machine is switched off when the fracture occurs and the distance between the upper testing jig and the lower testing jig becomes 10 mm larger than the position at the maximum load.

### 3. Definition of nominal stress

#### 3.1. Definition of nominal stress for the outer plate

Consider how to define the nominal stress for press-fitting structures suitable for designing the roller chains. Fig. 5(a-1) shows the stress distribution  $\sigma_\theta(r)$  when the pin is press-fitted into the outer plate. As shown in Fig. 5(a-1), due to the press-fitting, the compressive stress  $\sigma_\theta(r) < 0$  (at  $r = 0 \sim d/2$ ) appears at the pin, and the tensile stress  $\sigma_\theta(r) > 0$  (at  $r = d/2 \sim W/2$ ) appears at the outer plate. They are balanced as shown in equation (1). Here,  $d$  is the hole diameter of the outer plate,  $W$  is the width of the outer plate.

$$-\int_0^{d/2} \sigma_\theta(r) dr = \int_{d/2}^{W/2} \sigma_\theta(r) dr \quad (1)$$

$$\int_0^{W/2} \sigma_\theta(r) dr = 0 \quad (2)$$

Fig. 5(a-2) illustrates the stress distribution when the outer plate with the press-fitted pin is subjected to the tensile load  $F$  from the pin. To clarify the nominal stress, although actually the tensile load  $F$  is applied from the pin, Fig. 5(a-2) illustrates when the holed outer plate is subjected to tensile load  $F$ . Since the load  $F$  is applied to the minimum cross section of the holed plate without the pin, the nominal stress  $\sigma_n$  of the outer plate is defined in equation (3). Here,  $A$  denotes the minimum cross section area of the outer plate expressed by  $A = (W - d)t$  where  $t$  denotes the thickness of the outer plate.

$$\sigma_n = \frac{F}{A} = \frac{F}{(W - d)t} \quad (3)$$

#### 3.2. Definition of nominal stress for the inner plate

Regarding the nominal stress for the inner plate, the press-fitted bush should be considered. Fig. 5(b-1) illustrates the stress distribution  $\sigma_\theta(r)$  when the bush is press-fitted into the inner plate. As shown in Fig. 5(b-1), due to the press-fitting, the compressive stress  $\sigma_\theta(r) < 0$  appears at the bush for  $r = D_{BI}/2 \sim D_{BI}/2 + t_1$ , and the tensile stress  $\sigma_\theta(r) > 0$  appears at the inner plate for  $r = D_{BI}/2 + t_1 \sim W/2$ . The resultants of those stresses are balanced as shown in equation (4). Here,  $D_{BI}$  denotes the inner diameter of the bush,  $t_1$  denotes the thickness of the bush,  $W$  denotes the width of the inner plate.

**Table 4**  
Number of cycles to failure for the outer plate  $\sigma_a$ : Stress amplitude,  $\theta_f$ : Position of fracture in Fig. 2.

$\delta/D_p$ [ $\times 10^{-3}$ ]	Specimen number	$\sigma_a$ [MPa]	$R = \sigma_{n \min}/\sigma_{n \max}$	Number of cycles to failure $N_f$ [ $\times 10^6$ ]	$\theta_f$ [deg]
9.5	9.5-1	170	0.036	2.52	110
	9.5-2	148	0.042	4.60	100
	9.5-3	148	0.042	1.63	80
	9.5-4	148	0.042	5.43	80
	9.5-5	148	0.042	5.28	120
	9.5-6	137	0.045	1.78	115
	9.5-7	137	0.045	10 (Not broken)	-
	9.5-8	137	0.045	10 (Not broken)	-
	9.5-9	126	0.049	10 (Not broken)	-
	9.5-10	104	0.058	10 (Not broken)	-
5.1	5.1-1	170	0.036	0.58	120
	5.1-2	148	0.042	3.96	120
	5.1-3	148	0.042	0.71	100
	5.1-4	148	0.042	0.16	115
	5.1-5	148	0.042	0.28	115
	5.1-6	137	0.045	0.71	120
	5.1-7	137	0.045	1.19	95
	5.1-8	137	0.045	2.33	120
	5.1-9	126	0.049	10 (Not broken)	-
	5.1-10	104	0.058	10 (Not broken)	-
2.5	2.5-1	148	0.042	0.21	120
	2.5-2	148	0.042	0.30	110
	2.5-3	137	0.045	0.24	100
	2.5-4	137	0.045	0.14	110
	2.5-5	137	0.045	0.25	120
	2.5-6	137	0.045	0.44	90
	2.5-7	126	0.049	10 (Not broken)	-
0	0-1	126	0.049	0.12	90
	0-2	104	0.058	0.38	95
	0-3	104	0.058	0.16	90
	0-4	82	0.073	0.39	95
	0-5	82	0.073	0.45	100
	0-6	71	0.083	0.50	95
	0-7	60	0.097	1.34	95
	0-8	60	0.097	1.40	85
	0-9	49	0.12	10 (Not broken)	-

$$-\int_{D_{BI}/2}^{D_{BI}/2+t_1} \sigma_\theta(r) dr = \int_{D_{BI}/2}^{W/2} \sigma_\theta(r) dr \quad (4)$$

$$\int_{D_{BI}/2}^{W/2} \sigma_\theta(r) dr = 0 \quad (5)$$

To clarify the stress distribution, although the real specimen is subjected to the tensile load from the pin, Fig. 5(b-2) illustrates when the tensile stress is applied to the plate directly. Note that the tensile load  $F$  is applied to the bush as well as the inner plate. In other words, the tensile load  $F$  from the pin is applied to the minimum cross section area  $A = (W - D_{BI})t$  where  $D_{BI}$  denotes the inner diameter of the bush and  $t$  denotes thickness of the inner plate. The nominal stress at the minimum cross section  $A$  under the tensile load  $F$  can be defined in equation (6).

$$\sigma_n = \frac{F}{A} = \frac{F}{(W - D_{BI})t} \quad (6)$$

In real roller chain, all portions including the bush are subjected to the tensile load  $F$  from the pin. However, in the previous studies [36], the nominal stress  $\sigma_n$  is defined in equation (7). This equation shows that only the inner plate excluding the bush is subjected to the tensile load  $F$ . This is partly because as shown in Fig. 5(b-2) the maximum stress  $\sigma_{max}$  appears at  $r = D_{BI}/2 + t_1$  at the inner plate hole. Here,  $t_1$  denotes thickness of the bush. Since equation (7) does not consider the tensile load  $F$  applied to the bush, the nominal stress is overestimated.

$$\sigma_n = \frac{F}{(W - D_{BI} - 2t_1)t} \quad (7)$$

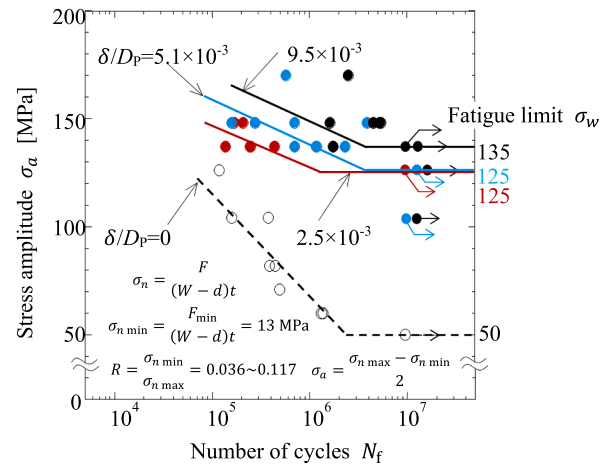
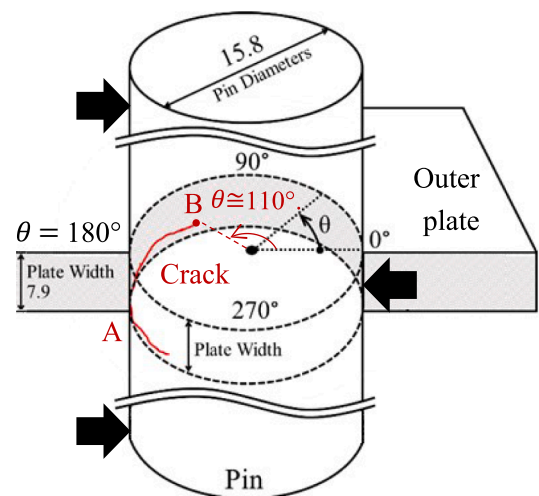
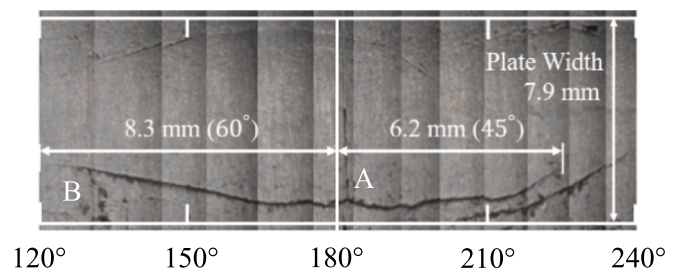


Fig. 6. S–N diagram for the outer plate specimen in Fig. 2(a).

By using the nominal stress newly defined in equation (6), the fatigue experiment is conducted under the cyclic loading  $F = F_{min} F_{max}$ . Here, the minimum load  $F_{min}$  is fixed as  $F_{min} = 3\text{kN}$  and the maximum load  $F_{max}$  is set as  $F_{max} = 25 \sim 80\text{kN}$ . Then, the minimum nominal stress is  $\sigma_{n \min} = 13\text{MPa}$  at  $F_{min} = 3\text{kN}$  and the maximum nominal stress  $\sigma_{n \max} = 110 \sim$



(a) Illustration of the cracked pin [mm]



(b) Crack observed on the pin surface

Fig. 7. Illustration of cracked pin when  $\delta/D_p = 9.5 \times 10^{-3}$  and  $\sigma_{n \max} = 265\text{ MPa}$ .

**Table 5**  
Cracked pin ratio for the pins press-fitted into the outer plate by varying  $\delta/D_p$ .

$\delta/D_p$ [ $\times 10^{-3}$ ]	Number of pins		Cracked pin ratio
	Number of pins investigated	Number of pins cracked	
9.5	16	14 (6*)	88 %
5.1	14	6	43 %
2.5	12	0	0 %
0	8	0	0 %

※ Among 14 pins, 6 pins are cracked even when the outer plates are not broken at the fatigue limit.

352 MPa at  $F_{max} = 25 \sim 80$  kN. The fatigue test is conducted at 9 levels in the range of the stress ratio  $R = \sigma_{n \min} / \sigma_{n \max} = 0.036 \sim 0.12$ .

#### 4. Experimental results and discussion

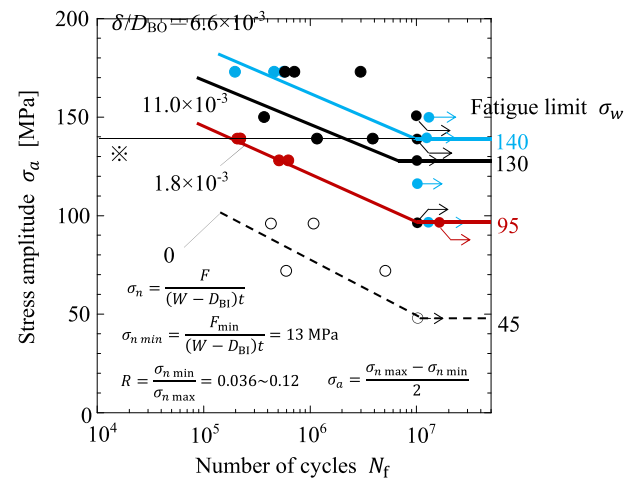
By varying the press-fitting ratio, the fatigue limit is discussed in terms of the stress amplitude  $\sigma_a = (\sigma_{n \max} - \sigma_{n \min}) / 2$  for the outer plate and the inner plate.

##### 4.1. Fatigue limit for the outer plate

Table 4 shows the number of cycles  $N_f$  to failure by varying the press-fitting ratio. The variation of  $N_f$  becomes larger at the larger press-fitting ratio. In Table 4, the position where the fatigue crack appears at the press-fitted portion defined as  $\theta$  in Fig. 2 is indicated as the position where the fracture happened as  $\theta = \theta_f$ . Table 4 shows the fracture position is in the range  $\theta_f = 80 \sim 120$  deg.

Fig. 6 shows the S–N diagram by varying the press-fitting ratio  $\delta/D_p$ . Under no press fitting  $\delta/D_p = 0$ , the fatigue limit  $\sigma_w = 50$  MPa but under press fitting when  $\delta/D_p \geq 2.5 \times 10^{-3}$  the fatigue limit becomes  $\sigma_w \cong 130$  MPa, which is more than twice of the fatigue limit when  $\delta/D_p = 0$ . The results show that the press-fitting is useful for improving the fatigue limit of roller chains. It should be noted that during the range  $\delta/D_p = 2.5 \times 10^{-3} \sim 9.5 \times 10^{-3}$ , the variation of the fatigue limit  $\sigma_w$  is small with  $< 8\%$ . It may be concluded that in real roller chains the press fitting ratio  $\delta/D_p = 9.5 \times 10^{-3}$  currently used should be reduced. If  $\delta/D_p$  is small, it can be press-fitted without applying oil to the fitting area. In this sense, a smaller press-fitting ratio is desirable because the same fatigue strength can be maintained, leading to a reduction in lubrication work. In this study, although the stress ratio  $R$  varies depending on the maximum load  $F_{max}$ , the values of  $R$  causing broken or not broken are approximately the same. For example, when the press-fitting ratio  $\delta/D_p = 9.5 \times 10^{-3}$ , Table 4 shows the specimen in Fig. 2(a) is broken when  $R = 0.036 \sim 0.045$ , and not broken when  $R = 0.045 \sim 0.058$ .

Under the larger press-fitting ratio  $\delta/D_p = 9.5 \times 10^{-3}$ , large scatter of  $N_f$  can be seen in Fig. 6 for the fatigue life. To find out the reason why the larger scatter appears, Fig. 7 illustrates an example of the crack observed at the pin when  $\delta/D_p = 9.5 \times 10^{-3}$  and  $\sigma_{n \max} = 265$  MPa. In Fig. 7(a), the point A denotes the origin of the crack, and the point B denotes the ending point of the crack at pin's surface. Table 5 shows that the cracked pin ratio increases with increasing the press-fitting ratio. When  $\delta/D_p$  is larger, cracks are usually observed at the pin although the outer plate is not fractured. As shown in Fig. 7(a), the maximum bending tensile stress for the pin appears at  $\theta = 180^\circ$ , which corresponds to the location of the fractured origin A of the outer plate. Fig. 7(b) shows a crack observed on the pin surface when  $\delta/D_p = 9.5 \times 10^{-3}$  and  $\sigma_{n \max} = 265$  MPa around  $\theta = 120^\circ \sim 240^\circ$  in the  $\theta$ -direction defined in Fig. 7. In the z-direction, the fractured origin A is located near the contact end surface of the outer plate's hole where the chamfer about 0.5 mm is provided. From the fracture origin A, the crack propagated diagonally toward the outer plate thickness center. From the fractured origin and the crack propagation direction, the crack can be identified as a typical fretting fatigue crack [37–42]. The fracture origin A corresponds to the crack initiation



※ Maximum load condition  $F_{max}$  used for analysis in Fig. 10

Fig. 8. S–N diagram for the inner plate specimen in Fig. 2(b).

of the pin because point A is located at the maximum bending stress and at the end of the contact surface. The ending point B of the crack at pin's surface corresponds to the crack initiation of the outer plate because point B is located near the fractured angle of the outer plate  $\theta_f \cong 110^\circ$ . As shown in Table 4, when the press-fitting ratio  $\delta/D_p = 5.1 \times 10^{-3}$ ,  $9.5 \times 10^{-3}$ , the fractured angle of the outer plate is  $\theta_f \cong 110^\circ$ .

As shown in Table 5, the cracked pin ratio increases with increasing the press-fitting ratio. When  $\delta/D_p = 9.5 \times 10^{-3}$ , among 16 pins investigated, 14 pins are cracked. Among 14 pins cracked, the cracks in 6 pins are observed without the final fracture of the outer plate at the fatigue limit. Therefore, it may be concluded that the pin is cracked before the outer plate is cracked and these fretting fatigue cracks at the pin affect the fractured origin controlling the life of the outer plate. When the pin and outer plate are assembled, the press-fitting at the room temperature is conducted by a human with a hammer. Therefore, it is difficult to reduce the variation in contact pressure between the pin and the outer plate due to the size of press-fitting scratches because there are variations in human work accuracy and the amount of oil adhered during press-fitting. In this way, the variation of  $N_f$  at the maximum press-fitting ratio  $\delta/D_p = 9.5 \times 10^{-3}$  is larger than the variation of  $N_f$  at the press-fitting ratio  $\delta/D_p = 0, 2.5 \times 10^{-3}, 5.1 \times 10^{-3}$ .

Almost the same fatigue limit during  $\delta/D_p = 2.5 \times 10^{-3} \sim 9.5 \times 10^{-3}$  in Fig. 6 is closely related to the cracked pin ratio, which increases with increasing  $\delta/D_p$  in Table 5. Due to the occurrence of fretting fatigue causing press-fit damage, the fatigue limit is affected largely. Instead, during  $\delta/D_p = 0 \sim 2.5 \times 10^{-3}$ , the fretting does not occur and the fatigue limit increases with increasing  $\delta/D_p$ . This can be explained from the reduction of the stress amplitude  $\sigma_{0a}$  as indicated in Table 7, which appears later regarding the inner plate. If such fretting fatigue cracks can be prevented, for example, by using a suitable measure such as introducing compressive residual stress at the pin's near-surface region, a large press-fitting ratio  $\delta/D_p \geq 9.5 \times 10^{-3}$  may improve the outer plate's fatigue strength significantly. This suggests that a significant improvement in fatigue strength can be expected in real roller chains by preventing the fretting fatigue.

Such large press-fitting ratio  $\delta/D_p \geq 9.5 \times 10^{-3}$  is commonly used in several roller chain makers. For example, regarding the inner plate, Nakagome et al [33] showed that the fatigue strength improved largely by using a large press-fitting ratio  $\delta/D_{BO} = 13.7 \times 10^{-3}$  compared to no press-fitting  $\delta/D_{BO} = 0$ . As shown in section 4.2 later, Fig. 8 also shows that the fatigue strength for the inner plate increases with increasing the press-fitting ratio except the maximum press-fitting ratio  $\delta/D_{BO} = 11.0 \times 10^{-3}$ . Regarding the outer plate, it should be noted that even if the pin is cracked but the outer plate is not broken, the damaged roller chains



**Table 6**  
Number of cycles to failure for the inner plate  $\sigma_a$ : Stress amplitude,  $\theta_f$ : Position of fracture in Fig. 2.

$\delta/D_{BO}$ [ $\times 10^{-3}$ ]	Specimen Number	$\sigma_a$ [MPa]	$R = \sigma_{n \min}/\sigma_{n \max}$	Number of cycles to failure $N_f$ [ $\times 10^6$ ]	$\theta_f$ [deg]
11.0	11.0-1	173	0.036	2.98	80
	11.0-2	173	0.036	0.58	90
	11.0-3	173	0.036	0.71	90
	11.0-4	150	0.041	0.37	100
	11.0-5	150	0.041	10 (Not broken)	-
	11.0-6	150	0.041	10 (Not broken)	-
	11.0-7	139	0.044	3.88	90
	11.0-8	139	0.044	1.16	105
	11.0-9	139	0.044	10 (Not broken)	-
	11.0-10	128	0.048	10 (Not broken)	-
	11.0-11	96	0.063	10 (Not broken)	-
	11.0-12	96	0.063	10 (Not broken)	-
6.6	6.6-1	173	0.036	0.57	90
	6.6-2	173	0.036	0.20	106
	6.6-3	173	0.036	0.46	90
	6.6-4	150	0.041	10 (Not broken)	-
	6.6-5	150	0.041	10 (Not broken)	-
	6.6-6	150	0.041	10 (Not broken)	-
	6.6-7	139	0.044	10 (Not broken)	-
	6.6-8	139	0.044	10 (Not broken)	-
	6.6-9	117	0.052	10 (Not broken)	-
	6.6-10	96	0.063	10 (Not broken)	-
1.8	1.8-1	139	0.044	0.22	98
	1.8-2	139	0.044	0.21	90
	1.8-3	139	0.044	0.22	110
	1.8-4	128	0.048	0.51	90
	1.8-5	128	0.048	0.62	100
	1.8-6	96	0.063	10 (Not broken)	-
	1.8-7	96	0.063	10 (Not broken)	-
0	0-1	96	0.063	1.07	80
	0-2	96	0.063	0.43	82
	0-3	72	0.082	0.60	95
	0-4	72	0.082	5.07	93
	0-5	47	0.12	10 (Not broken)	-

can be normal used in many cases. In this way, in real roller chains, a large press-fitting ratio is currently used although the pin is possibly cracked.

In this study, pin cracks due to fretting fatigue were newly found in the range of  $\delta/D_p = 5.1 \sim 9.5 \times 10^{-3}$ . However, only the slight difference of the fatigue limit can be seen when  $\delta/D_p = 2.5 \times 10^{-3} \sim 9.5 \times 10^{-3}$ . Therefore, using a smaller  $\delta/D_p$  can improve manufacturing efficiency without reducing fatigue strength. Also, to prevent cracking of the pin due to fretting fatigue, it is desirable that the press-fitting ratio  $\delta/D_p$  is small. In this way, it is necessary to reduce the press-fitting ratio  $\delta/D_p = 9.5 \times 10^{-3}$  currently used in real roller chains. The smaller press-fitting  $\delta/D_p < 9.5 \times 10^{-3}$  can be immediately applied to real roller chains.

#### 4.2. Fatigue limit for the inner plate

Table 6 shows the number of cycles to failure  $N_f$  by varying the press-

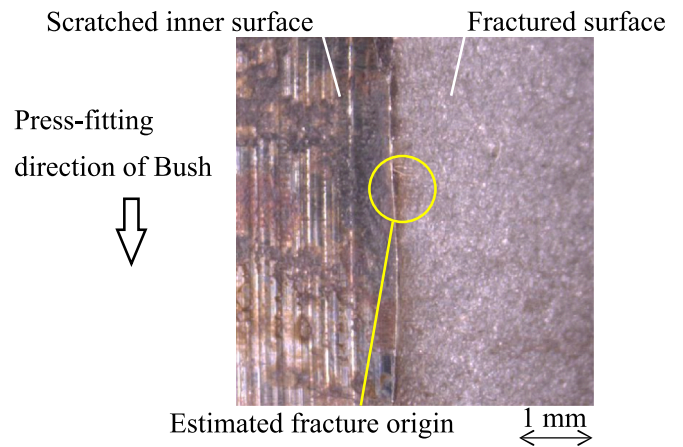


**Fig. 9.** Damaged hole surface of the inner plate due to press-fitting when  $\delta/D_{BO} = 11.0 \times 10^{-3}$  after fatigue testing.

fitting ratio. Fig. 6 shows the S–N diagram by varying the press-fitting ratio. In Table 6, the position where the fatigue crack appears at the shrink-fitted portion defined as  $\theta$  in Fig. 2 is indicated as the position where the fracture happened as  $\theta = \theta_f$ . Table 6 shows the fracture position is in the range  $\theta_f = 80 \sim 105\text{deg} \approx 90\text{deg}$ . Those angles coincide with the angles where the fracture occurs in a real roller chain. Therefore, in Section 5.2, the stress  $\sigma_\theta$  at  $\theta = 90\text{deg}$  will be mainly focused in the FEM analysis to identify the stress amplitude causing the fatigue fracture. The fatigue limit  $\sigma_w$  at the minimum press-fitting ratio  $\delta/D_{BO} = 1.8 \times 10^{-3}$  is 2.1 times larger than the fatigue limit  $\sigma_w$  at  $\delta/D_{BO} = 0$ . The fatigue limit  $\sigma_w$  at  $\delta/D_{BO} = 6.6 \times 10^{-3}$  is 3.1 times larger than the fatigue limit  $\sigma_w$  at  $\delta/D_{BO} = 0$ . The fatigue limit  $\sigma_w$  at the maximum press-fitting ratio  $\delta/D_{BO} = 11.0 \times 10^{-3}$  is lower than  $\sigma_w$  at  $\delta/D_{BO} = 6.6 \times 10^{-3}$ . The scatter of  $N_f$  at  $\delta/D_{BO} = 11.0 \times 10^{-3}$  is much larger than the other scatters at  $\delta/D_{BO} = 0, 1.8 \times 10^{-3}, 6.6 \times 10^{-3}$ . It may be concluded that the fatigue limit of the inner plate can be improved by the bush's press fitting ratio  $\delta/D_{BO} = 1.8 \times 10^{-3} \sim 11.0 \times 10^{-3}$  more than twice compared to  $\delta/D_{BO} = 0$ . In this study, although the stress ratio  $R$  varies depending on the maximum load  $F_{max}$ , the values of  $R$  causing broken or not broken are approximately the same. For example, when the press-fitting ratio  $\delta/D_{BO} = 11.0 \times 10^{-3}$ , Table 6 shows the specimen in Fig. 2(b) is broken when  $R = 0.036 \sim 0.044$ , and not broken when  $R = 0.041 \sim 0.063$ .

To investigate the reason why a larger scatter of  $N_f$  can be seen at  $\delta/D_{BO} = 11.0 \times 10^{-3}$  in Fig. 8, Fig. 9 shows the hole surface of the inner plate. As shown in Fig. 9, several scratches are caused by the bush press-fitting around the middle of the thickness. Since the fatigue crack may initiate from those scratches, the fatigue life of  $N_f$  at  $\delta/D_{BO} = 11.0 \times 10^{-3}$  varies depending on the dimension of the scratch. As described later in section 5.2, the FEM analysis shows that the fatigue strength increases with increasing the press-fitting ratio. When the bush and inner plate are assembled, the press-fitting at the room temperature is conducted by a human with a hammer. Therefore, it seems difficult to eliminate the large scratches due to the human work accuracy and the variation of the adhered oil amount and so forth. However, if such scratched damage can be prevented by using a proper method such as cold shrink-fitting where the bush is cooled down before shrink-fitting, the fatigue strength can be improved significantly for the inner plate by using a large value of  $\delta/D_{BO} \geq 11.0 \times 10^{-3}$ . After confirming the fatigue strength improvement, the cold shrink-fitting  $\delta/D_{BO} \geq 11.0 \times 10^{-3}$  can be immediately applied to real roller chains.

The fretting fatigue crack cannot be seen for the inner plate as well as the bush. The previous studies regarding the fretting fatigue showed under a large contact pressure and a large relative slip amplitude more cracks occur [37–42]. In the specimen in Fig. 2(b), the hollow bush is press-fitted into the inner plate, and the bush and the inner plate are

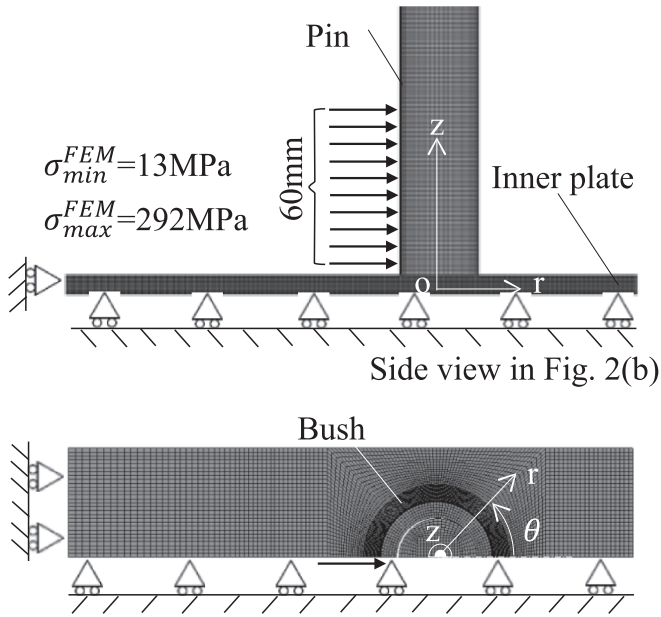


Fig. 10. FEM model and boundary conditions for the inner plate.

subjected to the tensile load  $F$  from the pin. Instead, in Fig. 2(a), the solid pin is press-fitted into the outer plate, and the outer plate is subjected to the tensile load  $F$  from the pin. It should be noted that under the same press-fitting ratio the press-fitting stress for the inner plate with the hollow bush is smaller than the press-fitting stress for the outer plate with the solid pin. Moreover, it should be noted the relative slip amount between the bush and the inner plate. The relative slip is caused by pin bending due to tensile load  $F$ . Since the relative slip of the pin bending does not directly affect the inner plate by the press-fitted bush, the relative slip amount between the inner plate's hole and the bush's outer diameter is smaller than the relative slip amount between the pin and the bush's inner diameter. Therefore, it may be concluded that the relative slip amount between the inner plate's hole and the bush's outer diameter is smaller than the relative slip amount between the outer plate's hole and the pin. Because of those reasons, the fretting fatigue crack does not occur for the inner plate.

## 5. Analytical results and discussion for the inner plate

### 5.1. Analytical method

The FEM analysis is performed to clarify the effect of the press-fitting ratio upon the fatigue strength. Regarding the outer plate, the fretting fatigue crack appearing at the pin may affect the fatigue strength of the outer plate. However, it is difficult to consider the fretting fatigue crack initiation and the propagation for the pin in the outer plate. Therefore, the inner plate will be considered to clarify the effect of the press-fitting ratio upon the fatigue strength by applying the FEM analysis.

Fig. 10 shows the FEM mesh for the 1/8 portion in Fig. 2(b) by considering the symmetry of the problem. The FEM mesh size is 0.1 ~ 1.2 mm for the inner plate, 0.5 mm for the bush, and 0.3 ~ 0.8 mm for the pin, and the total number of mesh is about  $0.9 \times 10^5$  mesh for the inner plate, about  $2.7 \times 10^3$  mesh for the bush, and about  $1.5 \times 10^5$  for the pin considering the material properties in Table 1 and the dimensions for each component in Fig. 2(b). The direct constraint method is applied for the contact analysis under the minimum nominal stress  $\sigma_{min}^{FEM} = 13$  MPa and the maximum nominal stress  $\sigma_{max}^{FEM} = 292$  MPa. The minimum nominal stress  $\sigma_{min}^{FEM} = 13$  MPa is set at the minimum load  $F_{min} = 3$  kN for the fatigue test. The maximum nominal stress  $\sigma_{max}^{FEM} = 292$  MPa is set at the maximum load  $F_{max} = 65$  kN when the fatigue limit shows the

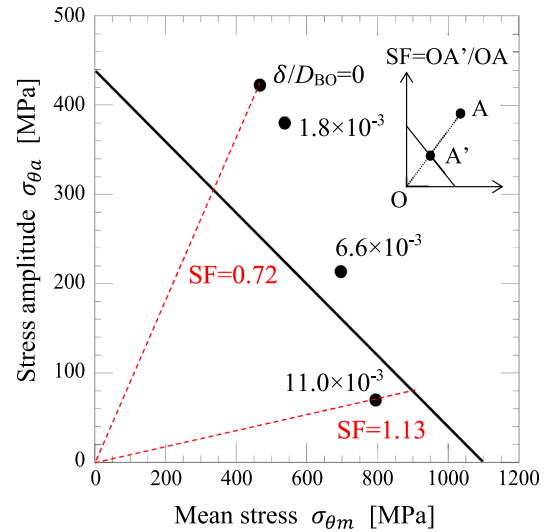


Fig. 11. Stress amplitude vs mean stress diagram for the inner plate.

maximum value at  $\delta/D_{BO} = 6.6 \times 10^{-3}$  in Fig. 8. Then, the three-dimensional elastic-plastic analysis is performed by using finite element method software MSC.MARC 2012 with hexahedral- 8-node isoparametric element. The press-fitting stress can be analyzed by adding the amount  $\delta$  to the bush's outer diameter contacting with the inner plate's hole.

### 5.2. Results and discussion

The authors previously analyzed that the total structure of the roller chain in Fig. 1 to compare the critical portions of each component [30]. The results showed that the circumferential stress  $\sigma_\theta$  for the inner/outer plate affects the fatigue fracture of the plate. Therefore, this study focuses on  $\sigma_\theta$  around the hole of the inner plate.

As shown in Table 6, the angle  $\theta_f$  specifying the crack initiation position at the inner plate's hole is always around  $\theta_f = 90^\circ$  regardless of the press-fitting ratio. Moreover, most of the fatigue crack initiated at the middle of the plate thickness where the chamfering does not affect. Therefore, in this FEM analysis, the position at the hole edge  $\theta = 90^\circ$  at the middle plate thickness at  $z = 0$  in Fig. 10 will be focused. Under the maximum press-fitting ratio  $\delta/D_{BO} = 11.0 \times 10^{-3}$ , the scratches due to press-fitting in Fig. 9 may affect the fracture origin. However, since the fatigue crack initiation angle  $\theta_f = 90^\circ$  at  $\delta/D_{BO} = 11.0 \times 10^{-3}$  is the same of the others. Therefore, four types of press-fitting ratios  $\delta/D_{BO} = 0, 1.8 \times 10^{-3}, 6.6 \times 10^{-3},$  and  $11.0 \times 10^{-3}$  are analyzed in a similar way.

Table 7 shows the minimum stress  $\sigma_{\theta min}$  under  $F = F_{min}$  and the maximum stress  $\sigma_{\theta max}$  under  $F = F_{max}$  by varying the press-fitting ratio. Here, the average stress  $\sigma_{\theta m}$  is defined as  $\sigma_{\theta m} = (\sigma_{\theta max} + \sigma_{\theta min})/2$ , and the stress amplitude  $\sigma_{\theta a}$  is defined as  $\sigma_{\theta a} = (\sigma_{\theta max} - \sigma_{\theta min})/2$ . The maximum stress  $\sigma_{\theta min}$  under  $F = F_{min}$  increases with increasing the press-fitting ratio  $\delta/D_{BO}$  because the external force effect  $F = F_{min} \cong 0$  is negligible and the shrink-fitting stress  $\sigma_\theta$  increases with increasing  $\delta/D_{BO}$ . Instead, the maximum stress  $\sigma_{\theta max}$  under  $F = F_{max}$  is almost constant regardless of the press-fitting ratio  $\delta/D_{BO}$  due to the combined effect of the external force and shrink-fitting.

To clarify the effect of the press-fitting ratio on the fatigue strength, Fig. 11 illustrates the stress amplitude vs the mean stress diagram. In Fig. 11, to express the fatigue limit line  $\sigma_a/\sigma_{w0} + \sigma_m/\sigma_B = 1$  for the plane specimen, the tensile strength  $\sigma_B = 1100$  MPa and the fully reversed fatigue limit  $\sigma_{w0} = 440$  MPa are obtained from Table 1. Here, the relative safety factor SF can be defined in equation (8) as indicated in Fig. 11.

$$SF = \overline{OA'}/\overline{OA} \quad (8)$$

Here, Point A denotes a FEM result of  $(\sigma_{\theta m}, \sigma_{\theta a})$  and Point A' denotes

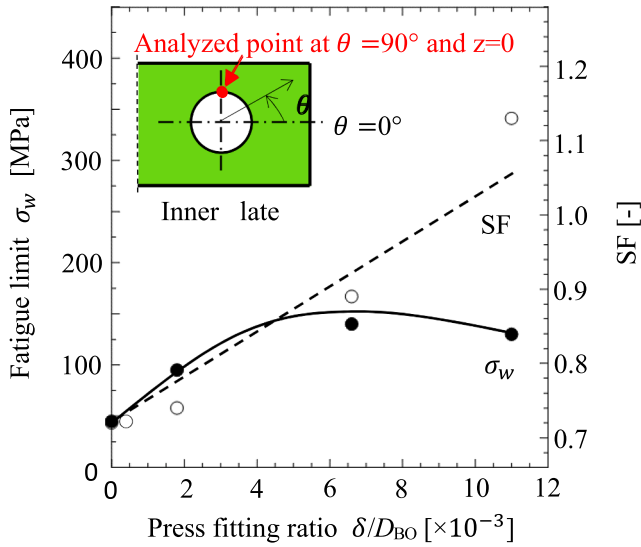


Fig. 12. Fatigue limit  $\sigma_w$  vs  $\delta/D_{BO}$  in comparison with SF vs  $\delta/D_{BO}$ .

the intersection of  $\overline{OA}$  line and the fatigue limit line  $\sigma_a/\sigma_{w0} + \sigma_m/\sigma_B = 1$ . Although the FEM result of  $(\sigma_{\theta m}, \sigma_{\theta a})$  only consider the point stress and does not consider the stress gradient, a larger SF value means the point is relatively safer than another point having a smaller SF value. As shown in Table 7 and Fig. 11, although the mean stress  $\sigma_{\theta m}$  increases with increasing the press-fitting ratio  $\delta/D_{BO}$ , the stress amplitude  $\sigma_{\theta a}$  decreases with increasing  $\delta/D_{BO}$ . This is the reason why the SF increases and the fatigue strength can be improved with increasing  $\delta/D_{BO}$ .

Fig. 12 shows the fatigue limit  $\sigma_w$  and the relative safety factor SF by varying the press-fitting ratio. Here, SF range in the y-axis is adjusted to compare SF with the fatigue limit  $\sigma_w$ . In Fig. 12, SF increases almost linearly from the minimum value at  $\delta/D_{BO} = 0$ . Therefore, the FEM analysis shows that the press-fitting is useful for improving the fatigue limit. However, the large difference can be seen between  $\sigma_w$  and SF at the press-fitting ratio  $\delta/D_{BO} = 11.0 \times 10^{-3}$ . As shown in section 4.2, the press-fitting scratch affects the fatigue strength  $\delta/D_{BO} = 11.0 \times 10^{-3}$  as the large scatter of  $N_f$ . It is conjectured that the FEM analysis without considering such scratches causes the difference between  $\sigma_w$  and SF at  $\delta/D_{BO} = 11.0 \times 10^{-3}$ .

## 6. Comparison of fatigue limit between the outer plate and the inner plate

In the previous sections, the fatigue strength of the outer and inner plates was discussed independently. However, the fatigue strength of the whole roller chains is controlled by the lower fatigue strength of the outer and inner plates. Therefore, it is essential to compare the fatigue strength of the outer and inner plates in the machine design of the roller chain since no study is available. As shown in Fig. 13(a), the solid pin is press-fitted into the outer plate hole. In contrast, as shown in Fig. 13(b), the hollow bush is press-fitted into the inner plate hole. Due to this difference, the press-fitted stress for the outer plate is larger than the press-fitted stress for the inner plate under the same press-fitting ratio.

In this study, the nominal stress  $\sigma_n$  is defined on the basis of the minimum cross section area  $A$  which is subjected to the tensile load  $F$  excluding the pin's cross where  $F$  is applied. For the outer plate, the minimum cross section area  $A$  is defined as  $A = (W - d)t$  where  $d$  denotes the hole diameter of the outer plate,  $W$  denotes the width of the outer plate, and  $t$  denotes the thickness of the outer plate. For the inner plate, the minimum cross section area  $A$  is defined as  $A = (W - D_{BI})t$  where  $D_{BI}$  denotes the inner diameter of the bush,  $W$  denotes the width of the inner plate,  $t$  denotes the thickness of the inner plate. The fatigue results should be considered on the basis of the nominal stress  $\sigma_n$  with the minimum cross section area  $A$ .

Table 8 and Fig. 14 show the fatigue limit  $\sigma_w$  by varying the press-fitting ratio. For reference, the y-axis on the right side of Fig. 14 shows the maximum load  $F_{max}$ . The fatigue limit  $\sigma_w$  of the inner plate coincides with the fatigue limit  $\sigma_w$  of the outer plate within 12 % independent of the press-fitting ratios  $\delta/D_P$  and  $\delta/D_{BO}$ .

As mentioned earlier, the outer and inner plates are made of the same

Table 7

Maximum stress  $\sigma_{\theta \max}$  and minimum stress  $\sigma_{\theta \min}$ , mean stress  $\sigma_{\theta m}$  and stress amplitude  $\sigma_{\theta a}$  for the inner plate at  $\theta = 90^\circ$  and  $z = 0$  [MPa].

$\delta/D_{BO}$ [ $\times 10^{-3}$ ]	$\sigma_{\theta \min}$ at $F = F_{min}$	$\sigma_{\theta \max}$ at $F = F_{max}$	$\sigma_{\theta m}$	$\sigma_{\theta a}$	SF
0	44	889	466.5	422.5	0.72
1.8	156	917	536.5	380.5	0.74
6.6	483	910	696.5	213.5	0.89
11.0	725	865	795.0	70.0	1.13

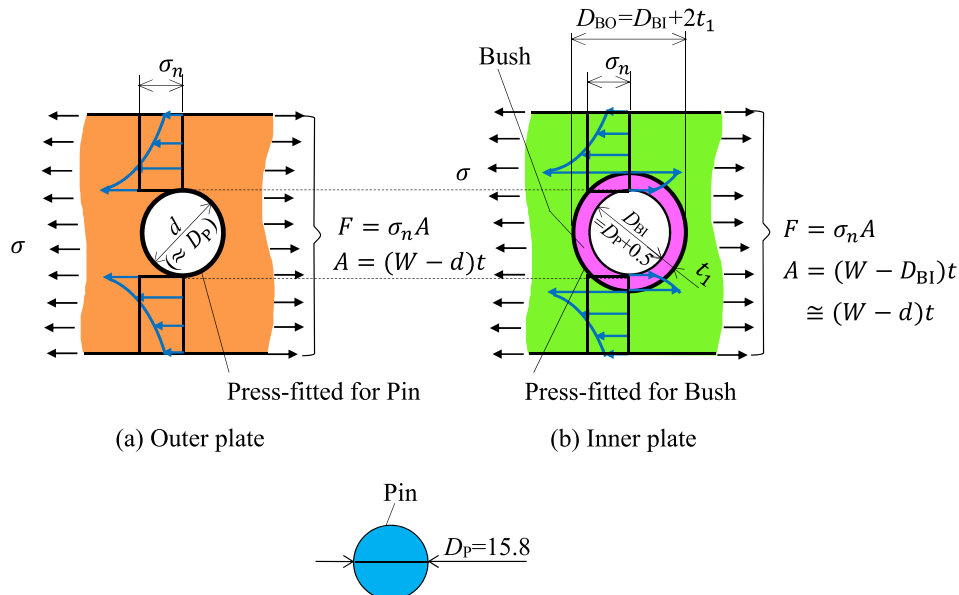
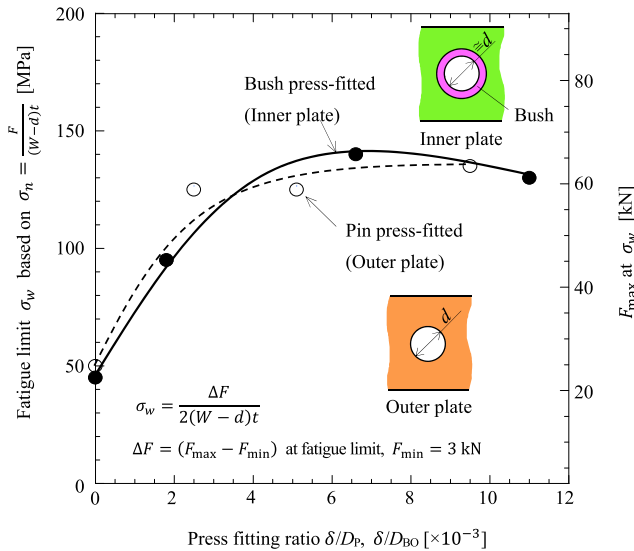


Fig. 13. Definition for nominal stress  $\sigma_n$ (unit: mm).

**Table 8**

Fatigue limit  $\sigma_w$  of the outer plate with press-fitted pin and the inner plate with press-fitted bush.

$\delta/D_p, \delta/D_{BO} [\times 10^{-3}]$	0	1.8	2.5	5.1	6.6	9.5	11.0
$\sigma_w$ of the outer plate in Fig. 6 [MPa]	50	—	125	125	—	135	—
$\sigma_w$ of the inner plate in Fig. 8 [MPa]	45	95	—	—	140	—	130



**Fig. 14.** Fatigue limit  $\sigma_w$  of the outer and inner plates based on the nominal stress  $\sigma_n$  with the minimum cross section area  $A$  excluding the pin's cross where  $F$  is applied.

material and the same lot, they have the same fatigue strength  $\sigma_w$ . As shown in Fig. 14, if the nominal stress  $\sigma_n$  in equation (6) is used with the same allowable stress, the same design load  $F$  can be obtained from the outer and inner plates. On the other hand, if the conventional nominal definition  $\sigma'_n$  in equation (7) is used with the same allowable stress, the design load from the inner plate is set lower since the bush in the inner plate does not bear the tensile load  $F$  and the nominal stress is calculated higher as  $\sigma'_n > \sigma_n$ . In this way, a nominal stress formula providing almost the same fatigue limit  $\sigma_w$  of the inner and outer plates as shown in Fig. 14 can be used usefully and conveniently for designing the outer and inner plates of a roller chain since the fatigue limits  $\sigma_w$  of the inner plate coincides with the fatigue limits of the outer plate within 12%. By using the new nominal stress formula (6) instead of the conventional definition (7), it is possible to reduce the dimensions of the inner plate and set the design load of the roller chain higher. A newly defined nominal stress can be immediately applied to the machine design of real roller chains.

**7. Conclusions**

Although great efforts have been done to improve the fatigue strength of roller chains, fatigue failure still happened mainly at the link plate's holes where the bush and pin are press-fitted. In this study, therefore, the fatigue experiment was conducted by using the specimens reflecting the outer/inner plates with press fitted pin/bush since they are controlling the whole strength of the roller chain. In real roller chains, the maximum stress amplitude appears from the tensile loading state and the press-fitting unloading state during the operation. Considering the difference of those two states, the fatigue experiment was conducted under pulsating alternative loading. The fatigue strength of the inner plate was compared with the outer plates with the aid of the FEM

analysis to clarify the effect of press-fitting on the fatigue strength. The conclusions can be summarized in the following way.

- (1) Considering the loading status of real roller chains, the fatigue experiment was conducted under pulsating alternative loading. From the specimen reflecting the inner plate of the real roller chain, it was confirmed that the bush's press-fitting when  $\delta/D_{BO} = 1.8 \times 10^{-3} \sim 11.0 \times 10^{-3}$  improves the fatigue limit by more than twice compared to no press-fitting  $\delta/D_{BO} = 0$ . At the largest press-fitting ratio  $\delta/D_{BO} = 11.0 \times 10^{-3}$ , the fatigue strength is reduced largely by the scratches observed along the hole although the fretting fatigue crack cannot be seen for the inner plate.
- (2) Regarding the inner plate, the FEM analysis clarified that with increasing the press-fitting ratio, the stress amplitude  $\sigma_{oa}$  decreases largely although the mean stress  $\sigma_{om}$  increases. This is reason why the fatigue strength can be improved by the press-fitting for real roller chains. If the scratched damage can be prevented by using a proper method like cold shrink-fitting by cooling the bush instead of the press-fitting currently, the fatigue strength of the inner plate can be improved significantly by using a larger cold shrink-fitting ratio  $\delta/D_{BO} \geq 11.0 \times 10^{-3}$ . After confirming the fatigue strength improvement, the cold shrink-fitting  $\delta/D_{BO} \geq 11.0 \times 10^{-3}$  can be immediately applied to real roller chains.
- (3) Regarding the outer plate, the fatigue experiment considering the loading status of real roller chains confirmed that the press-fitting is also useful since the fatigue limit can be improved by the press-fitted pin more than twice compared to no press-fitting  $\delta/D_p = 0$ . However, only the slight difference can be seen for the press fitting ratio  $\delta/D_p = 2.5 \times 10^{-3} \sim 9.5 \times 10^{-3}$ . Therefore, the manufacturing efficiency can be improved by using smaller  $\delta/D_p$  without reducing the fatigue strength. The press-fitting ratio  $\delta/D_p = 9.5 \times 10^{-3}$  currently used in real roller chains should be reduced. The smaller press-fitting  $\delta/D_p < 9.5 \times 10^{-3}$  can be immediately applied to real roller chains.
- (4) Even when the outer plate is not finally fractured at a large press-fitting ratio  $\delta/D_p = 9.5 \times 10^{-3}$ , a large crack can be seen in the pin due to the fretting fatigue. These fretting fatigue cracks observed at the pin largely reduce the fatigue strength by affecting the fractured origin of the outer plate. However, by using a suitable measure such as introducing a compressive residual stress at the pin's near-surface region to prevent such fretting fatigue region, a large press-fitting ratio  $\delta/D_p \geq 9.5 \times 10^{-3}$  may improve the outer plate's fatigue strength largely. This suggests that a significant improvement in fatigue strength can be expected in real roller chains by preventing the fretting fatigue.
- (5) A newly defined nominal stress  $\sigma_n$  was proposed in this paper since the nominal stress  $\sigma'_n$  in the previous studies does not take into account that the bush supports part of the tensile load  $F$ . The results showed that the newly defined nominal stress  $\sigma_n$  can be used usefully and conveniently since the fatigue limits of the inner plate coincides with fatigue limits of the outer plate within 12% independent of the press-fitting ratio. By using the new nominal stress formula (6) instead of the conventional definition (7), it is possible to reduce the dimensions of the inner plate and set the design load of the roller chain higher. A newly defined nominal stress can be immediately applied to machine design of real roller chains.

**Declaration of Competing Interest**

The authors declare that they have no known competing financial interests or personal relationships that could have appeared to influence the work reported in this paper.



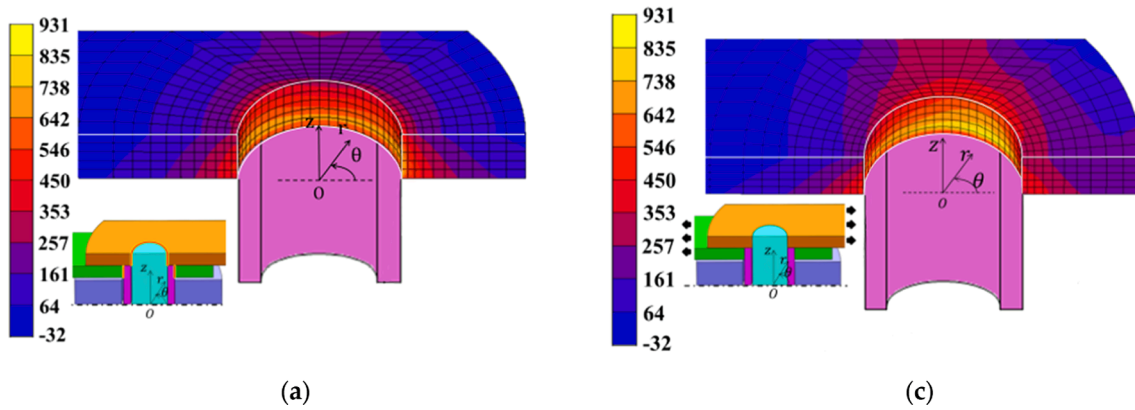


Fig. A1. Stress distribution  $\sigma_\theta$  for the inner plate in Fig. 1 [MPa]: (a) press-fitting state; (c) tensile state.

## Data availability

No data was used for the research described in the article.

## Appendix A.: Stress $\sigma_\theta$ appearing at outer and inner plates in real roller chain during operation

Fig. A1 illustrates the stress distribution  $\sigma_\theta$  for the inner plate in Fig. 1 under (a) press-fitting state, and (c) tensile state. As shown in Fig. A1(a), although no external force is applied in (a) press-fitting state, the tensile stress distribution  $\sigma_\theta$  appears due to the press-fitting of the bush into the inner plate. Also, as shown in Fig. A1(c), due to the tensile loading after the press-fitting, the larger tensile stress distribution  $\sigma_\theta$  appears at the tensile state of the inner plate. The difference between those figures can be regarded as the stress amplitude causing metal fatigue of the inner plate.

## References

- Pereira CM, Ambrosio JA, Ramalho AL. A methodology for the generation of planar models for multibody chain drives. *Multibody SysDyn* 2010;24:303–24. <https://doi.org/10.1007/s11044-010-9207-x>.
- Wragge-Morley R, Yon J, Lock R, Alexander B, Burgess S. A novel pendulum test for measuring roller chain efficiency. *Meas Sci Technol* 2018;29(7). <https://doi.org/10.1088/1361-6501/aaa239>.
- Zheng H, Wang YY, Quek KP. A refined numerical simulation on dynamic behavior of roller chain drives. *Shock Vib* 2004;11:573–84. <https://doi.org/10.1155/2004/548172>.
- Wasan S, Chakrit S. An integrating finite element method and multi-body simulation for drive systems analysis. *Eng J* 2017;21(1):221–34. <https://doi.org/10.4186/ej.2017.21.1.221>.
- Sine LP, John MH, Jorge ACA. A roller chain drive model including contact with guide-bars. *Multibody SysDyn* 2004;12:285–301. <https://doi.org/10.1023/B:MUBO.0000049131.77305.d8>.
- Ambrosio J, Malça C, Ramalho A. Cylindrical contact force models for the dynamics of roller chain drives. *Multibody Mechatronic Syst* 2015;25:121–31. [https://doi.org/10.1007/978-3-319-09858-6\\_12](https://doi.org/10.1007/978-3-319-09858-6_12).
- Xu L, Yang Y, Chang Z, Liu J. Dynamic modeling of a roller chain drive system considering the flexibility of input shaft. *Chinese Journal of Mech Eng* 2010;23(3):367–74. <https://doi.org/10.3901/CJME.2010.03.367>.
- Niels F, Jon JT. Kinematic and dynamic modeling and approximate analysis of a roller chain drive. *J Sound Vib* 2016;366(13):447–70. <https://doi.org/10.1016/j.jsv.2015.12.028>.
- Niels F, Jon JT. Kinematics of roller chain drives - exact and approximate analysis. *Mech Mach Theory* 2016;100:17–32. <https://doi.org/10.1016/j.mechmachtheory.2016.01.009>.
- Pedersen SL. Model of contact between rollers and sprockets in chain-drive systems. *Arch Appl Mech* 2005;74:489–508. <https://doi.org/10.1007/s00419-004-0363-4>.
- Xu L, Li Y. Numerical simulation on dynamic behavior of intermittent roller chain drives. *Appl Mech Mater* 2012;155:535–9. <https://doi.org/10.4028/www.scientific.net/AMM.155-156.535>.
- Ambrosio J, Malça C, Ramalho A. Planar roller chain drive dynamics using a cylindrical contact force model. *Mech Based Des Struct Mach* 2016;44(1):109–22. <https://doi.org/10.1080/15397734.2015.1087319>.
- Pedersen SL. Simulation and analysis of roller chain drive systems, No. S 92. Technical University of Denmark. DCAMM Report; 2004.
- Lu P. Supplement of several problems in roller chain drive design. *Adv Mat Res* 2013;774:176–9. <https://doi.org/10.4028/www.scientific.net/AMR.774-776.176>.
- Li B, Fan S, Zhang Y. The modal analysis of roller chain drives. *Adv Mat Res* 2011;291:1551–4. <https://doi.org/10.4028/www.scientific.net/AMR.291-294.1551>.
- Reddy YMM, Chander PR. Fatigue analysis of chain sprocket using finite element analysis. *Int J Adv Eng Res Development* 2018;5(4):917–22. e-ISSN (O): 2348–4470.
- Wang Y, Ji D, Zhan K. Modified sprocket tooth profile of roller chain drives. *Mech Mach Theory* 2013;70:380–93. <https://doi.org/10.1016/j.mechmachtheory.2013.08.006>.
- Bhoite TD, Pawar PM, Gaikwad BD. Fea Based Study of effect of radial variation of outer link in a typical roller chain link assembly. *international Journal of Mechanical and Industrial Engineering* 2012;1(4):65–70. <https://doi.org/10.47893/IJMIE.2012.1070>.
- Noguchi S, Nagasaki K, Nakayama S, Kanada T, Nishino T, Ohtani T. Static stress analysis of link plate of roller chain using finite element method and some design proposals for weight saving. *J Adv Mechat Design, Syst Manuf* 2009;3(2):159–70. <https://doi.org/10.1299/jamds.3.159>.
- Xu S, Wang Y, Meng F. Study on the reliability evaluation method of the wear life of roller chains. *J Mech Eng Sci* 2006;220(10):1569–74. <https://doi.org/10.1243/0954406JMES235>.
- Zhao JT, Wang SZ, Wang ZX. The effects of the wear elongation on the load of a Long-distance transmission chain. *Appl Mech Mater* 2013;456:60–4. <https://doi.org/10.4028/www.scientific.net/AMM.456.60>.
- Zhang Y, Yang Z, Li D. The roller chain lubricated with ferrofluids. *Journal of Engineering, Tribology* 2019;233(6):927–35. <https://doi.org/10.1177/1350650118806799>.
- Goran R, Vesna A, Vlatko M. Study of stainless steel resistance in conditions of tribocorrosion wear. *interdisciplinary description of. Complex Systems* 2015;13(3):461–71. <https://doi.org/10.7906/index.13.3.10>.
- Bressan JD, Daros DP, Sokolowski A, Mesquita RA, Barbosa CA. Influence of hardness on the wear resistance of 17–4 PH stainless steel evaluated by the pin-on-disc testing. *J Mater Process Technol* 2008;205(1):353–9. <https://doi.org/10.1016/j.jmatprotec.2007.11.251>.
- Krishnakumar K, Arockia SA. A Review of failure analysis found in industrial roller chains. *Int J ChemTech Res* 2015;8(12):598–603. URL: [https://sphinxsai.com/2015/ch\\_vol8\\_no12/3/\(598-603\)V8N12CT.pdf](https://sphinxsai.com/2015/ch_vol8_no12/3/(598-603)V8N12CT.pdf).
- Jagtap MD, Gaikwad BD, Pawar PM. Study of roller conveyor chain strip under tensile loading. URL: [https://www.academia.edu/7652516/Study\\_of\\_Roller\\_Conveyor\\_Chain\\_Strip\\_under\\_Tensile\\_Loading](https://www.academia.edu/7652516/Study_of_Roller_Conveyor_Chain_Strip_under_Tensile_Loading).
- Kim C, Chung J, Song J. Dynamic analysis of long heavy-duty roller chain for bucket elevator of continuous ship unloader. *Adv Mech Eng* 2017;9(8):1–11. <https://doi.org/10.1177/1687814017723296>.
- Zhang S, Tak T. Efficiency estimation of roller chain power transmission system. *Appl Sci* 2020;10(21). <https://doi.org/10.3390/app10217729>.
- Amiruddin H, Abdollah MFB, Mohamad Nizar MAD. Measurement of roller chain wear lubricated with palm oil-based hexagonal boron nitride nanoparticles. *Industrial Lubrication and Tribol* 2020;72(10):1199–204. <https://doi.org/10.1108/ILT-02-2020-0061>.



- [30] Saito R, Noda N-A, Sano Y, Song J, Minami T, Birou Y, et al. Fatigue strength analysis and fatigue damage evaluation of roller chain. *Metals* 2018;8(10):847–61. <https://doi.org/10.3390/met8100847>.
- [31] Saito R, Noda N-A, Sano Y. Newly developed wear testing machine having sufficient reproducibility useful for investigating roller chains. *ISIJ Int* 2020;60(10):2255–65. <https://doi.org/10.2355/isijinternational.ISIJINT-2020-086>.
- [32] Mizuno M. The effect of number of pitches of test pieces on the fatigue life of roller-chains. *Proceedings of the Fujihara Memorial Faculty of Engineering, Keio University*; 1961; p. 146–153. URL: [https://koara.lib.keio.ac.jp/xoonips/modules/xoonips/detail.php?koara\\_id=KO50001004-00140055-0026&ml\\_lang=ja](https://koara.lib.keio.ac.jp/xoonips/modules/xoonips/detail.php?koara_id=KO50001004-00140055-0026&ml_lang=ja).
- [33] Nakagome M, Mizuno M. “Effects of pre-loading and press-fit of bushings to the fatigue strength of roller chain link-plates. *J Soc Prec Eng* 1977;43(514):1161–6. <https://doi.org/10.2493/jjspe1933.43.1161>.
- [34] Kawamoto M, Yukawa A. Fatigue strength of an eye-end with press fit. *J Soc Test Mater* 1954;3(17):439–42. <https://doi.org/10.2472/jsms1952.3.439>.
- [35] Naraki M., Noguchi S. *Proceedings on the 2011 Conference on Design Engineering and Science. JSDE*; 2011; p. 121-122.
- [36] Aoi S. *Chain Conveyor [Conveyor Series 2]. Ltd, Tokyo: Yakumoshoten Co.; 1958.*
- [37] Wang W, Wang M, Yang G, Xie J. Experimental investigation of fretting fatigue of train axles under rotating bending. *Adv Mat Res* 2011;291:1110–5. <https://doi.org/10.4028/www.scientific.net/AMR.291-294.1110>.
- [38] Gurer G, Gur CH. Failure analysis of fretting fatigue initiation and growth on railway axle press-fits. *Eng Fail Anal* 2018;84:151–66. <https://doi.org/10.1016/j.engfailanal.2017.06.054>.
- [39] Siegfried F, Philippe K, Leo V. Quantification of fretting damage. *Wear* 1996;200(1):186–205. [https://doi.org/10.1016/S0043-1648\(96\)07306-1](https://doi.org/10.1016/S0043-1648(96)07306-1).
- [40] Steven C. Fatigue properties of railway axles: New results of full-scale specimens from Euraxles project. *Int J Fatigue* 2016;86:2–12. <https://doi.org/10.1016/j.ijfatigue.2015.11.028>.
- [41] Chowdhury MA, Kowser MA, Zobaer Shah QM, Das S. Characteristics and damage mechanisms of bending fretting fatigue of materials. *Int J Damage Mech* 2017;27(4). <https://doi.org/10.1177/1056789517693412>.
- [42] Mutoh Y. Fracture mechanisms of fretting fatigue. *J Soc Mater Sci* 1997;46(11):1233–41. <https://doi.org/10.2472/jsms.46.1233>.
- [43] Hamada S, Sakoda Y, Sasaki D, Ueda M, Noguchi H. Evaluation of fatigue limit characteristics of lamellar pearlitic steel in consideration of microstructure. *J Soc Mater Sci* 2011;60(9):790–5. <https://doi.org/10.2472/jsms.60.790>.